Letter

Chiral spin liquids with projected Gaussian fermionic entangled pair states

Sen Niu [1,*] Jheng-Wei Li [2] Ji-Yao Chen [3,†] and Didier Poilblanc [1,‡]

[1]*Laboratoire de Physique Théorique, C.N.R.S. and Université de Toulouse, 31062 Toulouse, France*

[2]*Université Grenoble Alpes, CEA, Grenoble INP, IRIG, Pheliqs, F-38000 Grenoble, France*

[3]*Guangdong Provincial Key Laboratory of Magnetoelectric Physics and Devices, Center for Neutron Science and Technology, School of Physics, Sun Yat-sen University, Guangzhou 510275, China*

(Received 20 July 2023; revised 3 October 2023; accepted 23 January 2024; published 12 February 2024)

We study the parton construction of chiral spin liquids (CSLs) using projected Gaussian fermionic entangled pair states (GfPEPSs). First, we show that GfPEPSs can represent generic spinless Chern insulators faithfully with finite bond dimensions. Then by applying the Gutzwiller projection to a bilayer GfPEPSs, spin-$\frac{1}{2}$ Abelian and non-Abelian CSLs are obtained for Chern number $C = 1$ and 2, respectively. As a consequence of the topological obstruction for GfPEPSs, very weak Gossamer tails are observed in the correlation functions of the fermionic projected entangled pair state (PEPS) *Ansätze*, suggesting that the no-go theorem for chiral PEPS is universal but does not bring any practical limitation. Remarkably, without finetuning, all topological sectors can be constructed showing the expected number of chiral branches in the respective entanglement spectra, providing a sharp improvement with respect to the known bosonic PEPS approach.

DOI: 10.1103/PhysRevB.109.L081107

Introduction. The notion of the topological phase has revolutionized our understanding of phases of matter beyond the Landau paradigm. In two-dimensional systems without time-reversal symmetry, if there exist chiral edge modes moving only in one direction, the states are dubbed chiral topological states. The most well-known chiral state in lattice-free fermion systems is the Chern insulator [1,2], where the topology is completely characterized by the bulk Chern number C indicating the number of chiral edge modes [3,4]. Through Gutzwiller projection on copies of Chern insulators (labeled by a spin index), a chiral spin-liquid (CSL) state in the parton representation [5] can be obtained. Interestingly, in contrast with their parent chiral Chern insulators, CSLs inherit long-range entanglement from the Gutzwiller projection. Hence, CSLs are bosonic variants of the fractional quantum Hall states and can be classified by the chiral gapless modes on the edge or, equivalently, the entanglement spectrum (ES) [6,7] described by (1+1)-dimensional conformal field theories (CFTs) [8]. For example, for two copies of half-filled Chern insulators with $C = 1$ in each copy, the projected spin state becomes the topological $SU(2)_1$ CSL [9,10] which is equivalent to the bosonic $\nu = \frac{1}{2}$ Laughlin wave function [11]. In more general cases, the topological nature of parton wave functions built from Chern insulators with higher Chern number are not clear. For conventional methods like variational Monte Carlo [12], computation of the ES of projected parton states is very involved and, hence, has been achieved only in very rare specific cases [13]. Thus, characterizing parton wave functions through entanglement-based methods, e.g., projected entangled pair states (PEPSs) [14], is desired.

PEPSs have been successfully used for investigating two-dimensional topological states, where nonchiral topological orders can be encoded by gauge symmetry exactly [15–18]. However, there seems to exist a topological obstruction for PEPSs to represent chiral topological states. For the case of free fermions where the corresponding PEPS representation is the Gaussian fermionic PEPS (GfPEPS), the obstruction has been proven exactly [19–21], namely, if a GfPEPS is chiral, then its bulk should be gapless. For the non-Gaussian case such as those in spin systems, a series of numerical studies shows that the numerically optimized chiral bosonic PEPSs also have artificial (gossamer) long-range correlations in the bulk [22–25]. Since interacting chiral PEPSs are also likely to be subject to topological obstruction, it becomes important to scrutinize the possible artifacts of the PEPS descriptions of a true CSL. Do we have some sort of universality in its description in terms of bosonic and fermionic interacting PEPSs? More importantly, there exist several subtle issues in the numerically optimized bosonic PEPS, e.g., the existence of redundant chiral branches in the ES [24,26–28] and the challenge in accessing the complete set of topological sectors [23]. Thus, it is interesting to see whether the projected fermionic PEPS describes the edge theory of CSLs faithfully, which could also shed light on resolving the problems in bosonic PEPSs. For that purpose, we study generic chiral spin liquids using optimized GfPEPS parton wave functions constructed from a parent Chern insulator Hamiltonian [29].

GfPEPS for Chern insulator. As a preliminary step before constructing Gutzwiller-projected parton wave functions, we investigate the GfPEPS representations for free fermion Chern insulators. One representative lattice model is the two-band

*sen.niu@irsamc.ups-tlse.fr

†chenjiy3@mail.sysu.edu.cn

‡didier.poilblanc@irsamc.ups-tlse.fr

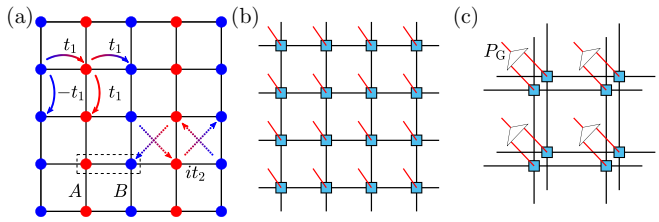

FIG. 1. Schematic diagrams of (a) the Hofstadter Chern insulator model with a two-site A, B unit-cell along the x direction marked by the dashed line, (b) the translation invariant GfPEPS *Ansatz* with A, B physical sites included in one tensor and (c) the spin state constructed from Gutzwiller-projected GfPEPSs.

Hofstadter model [30,31]:

$$H = -\sum_{m,n}(t_1 c^\dagger_{m+1,n}c_{m,n} + t_1 e^{im\pi} c^\dagger_{m,n+1}c_{m,n}) - \sum_{m,n}[t_2 e^{i(m\pi \pm \pi/2)} c^\dagger_{m\pm1,n+1}c_{m,n}] + \text{H.c.} \quad (1)$$

Here, (m, n) denotes the coordinates of the fermionic creation and annihilation operators, and the phases of hopping terms t_1, t_2 can be read from Fig. 1(a), providing a homogeneous $\pi/2$ flux in all triangular units. The sites can be relabeled with A, B sublattice indices as $c^\dagger_{2x-1,y} = c^\dagger_{x,y,A}$ and $c^\dagger_{2x,y} = c^\dagger_{x,y,B}$. At half-filling, the exact ground state is a gapped insulator with Chern number $C = 1$ for $t_1, t_2 > 0$. To simulate the free fermion ground state, we adopt the translation invariant particle number conserving U(1) symmetric GfPEPS *Ansatz* parametrized by a single tensor in Fig. 1(b) and perform variational optimization [32,33]. The translation invariant GfPEPS at half-filling can be written as a product state in the Brillouin zone, where all k modes are determined by the single real-space tensor and cannot vary independently. The cost function is chosen as the expectation value of Eq. (1) [33]. Here, a single tensor contains A, B physical sites of the unit-cell with a physical Hilbert space dimension $d = 2^2$ and virtual bond dimension $D = 2^M$, where M is the number of virtual fermionic modes. Thus, the one-site translation (projective) symmetry in the x direction is only approximately realized but can be improved with increasing M.

In the Hofstadter model, the optimized GfPEPS shows topological features when the number of virtual modes satisfies $M \geqslant M_{\min}$ and then becomes sharper with increasing M, as depicted in Fig. 2. We set $t_1 = 1$ and focus on the parameter $t_2 = 0.5$ with the largest band gap. Starting from $M = 1$, the energy error decreases systematically, see Fig. 2(a). The topology of the optimized free fermion states can be deduced from the number of chiral branches in the single-particle ES λ_α [34,35], or equivalently, from the edge spectrum $\epsilon_\alpha = (e^{\lambda_\alpha} + 1)^{-1}$ of the subsystem correlation matrix C^{cut}, defined as

$$C^{\text{cut}}_{i,j} = \begin{cases} \text{Tr}[|\psi\rangle\langle\psi|c^\dagger_i c_j], & i, j \in \text{subsystem}, \\ 0, & \text{otherwise}. \end{cases} \quad (2)$$

Here, $|\psi\rangle$ is the free fermion many-body state on the whole lattice. Along the y direction, we cut out a cylinder from the torus as a subsystem and plot the correlation matrix

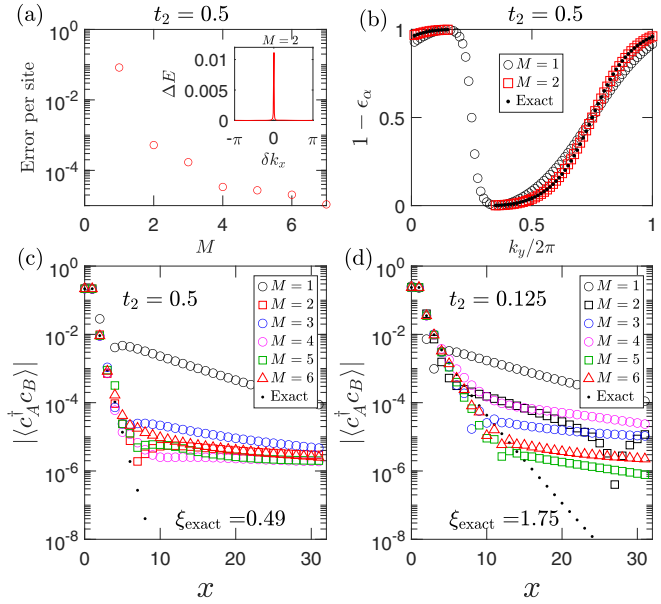

FIG. 2. Observables of the GfPEPS for the Hofstadter model optimized on a 80×80 torus. (a) Energy error per site vs M. Inset shows energy error along the k_x direction path across the sharp singular point in k space with $M = 2$. (b) Edge spectrum of the correlation matrix localized at one boundary of the 40×80 cylinder cut from the torus. (c) and (d) Correlation functions for different t_2 values. The open black circles correspond to trivial states without chirality.

spectrum ϵ_α in Fig. 2(b), where bulk states have been removed according to a numerical criterion $|\epsilon_\alpha - 0.5| > 0.499$. The $M = 1$ state is nonchiral since both left- and right-moving modes exist, while for $M \geqslant 2$, the dispersion of the edge mode becomes chiral and shows quantitative agreement with the exact results.

We then examine the real-space bulk correlation functions between A, B sublattices at distance x, defined as $\langle c^\dagger_A c_B\rangle = \langle c^\dagger_{1,y} c_{2x,y}\rangle$ (the exact correlation functions between the same sublattice always vanish). The corresponding GfPEPS results are shown in Fig. 2(c), where for $M \geqslant 2$, the optimized states with correct topology exhibit a crossover behavior: At short distance, the correlations decay exponentially as expected until approaching a small magnitude $\sim 10^{-5}$ and then show a weak long-distance gossamer tail with algebraic decay (which we have confirmed by fitting on much larger clusters). The existence of the long-distance tail can be understood from a sharp momentum space singular point, as shown in the inset of Fig. 2(a), and is consistent with the topological obstruction for GfPEPS. It is expected that the correlation functions improve as M increases, although in practice, the precision of our numerical optimization sets some limit. In Fig. 2(d), we show the results for $t_2 = 0.125$, exhibiting a much longer bulk correlation length and slower decay of correlations, from which one can roughly observe that the weight of the artificial gossamer tail decreases with M.

We find a different scenario for the optimized GfPEPS in another Chern insulator model—the Qi-Wu-Zhang model [36]. The minimal bond dimension to observe the chiral edge is $M = 1$, but in that case, there is no sharp singularity

in momentum space and no crossover behavior in correlation functions, akin to the family of states investigated in Refs. [19,20,37]. For larger bond dimensions $M > 1$, the same momentum and real-space behaviors as those in the Hofstadter model are observed. The corresponding numerical results are shown in the Supplemental Material (SM) [38].

Gutzwiller projected spin state with $C = 1$. We now move to the Gutzwiller projected state, which is expected to be the $SU(2)_1$ CSL when $C = 1$. By construction [33,37], we build the SU(2) invariant fermionic state via stacking two copies of GfPEPSs labeled by spin $\uparrow$ and $\downarrow$ components; hence, the tensors with virtual bond dimension 4^M satisfy $U(1)\times SU(2)$ symmetry, and each virtual state is labeled by both charge and spin quantum numbers. The tensor for the spin state is obtained by applying the Gutzwiller projector $P_G = \prod_i (\hat{n}_{i,\uparrow} + \hat{n}_{i,\downarrow})(2 - \hat{n}_{i,\uparrow} - \hat{n}_{i,\downarrow})$, as shown in Fig. 1(c). After grouping the double-layer virtual indices, the tensor can be treated as conventional PEPSs numerically. We choose the $M = 2$ GfPEPS optimized at $t_2 = 0.5$ and construct PEPS representation of the projected state using the fermionic tensors [39,40]. To inspect the real-space correlation functions on the infinite lattice, we use the corner transfer matrix renormalization group (CTMRG) [41,42] method, where the approximate contraction is controlled by the environment bond dimension χ and becomes exact in the $\chi \to \infty$ limit. The numerical results for spin-spin correlations $\langle \mathbf{S}_A \cdot \mathbf{S}_B \rangle$ between A, B sublattices at distance x are shown in Fig. 3(a). The correlations of the projected state decay also exponentially at short distance up to a length scale $x \approx 5$ and then decay much slower. As the absolute value of the slope at long distance decreases with χ, we expect the exact correlation function (which corresponds to the limit $\chi \to \infty$) of this $M = 2$ state decays slower than any exponential decay, like the correlations in chiral bosonic PEPSs [22–25].

The topological order of the CSL state is characterized by the bipartite ES, which can be computed on an infinitely long cylinder [43]. The topologically degenerate spin states can be constructed from projected free fermion states with different boundary conditions. The flux inserted by the antiperiodic boundary condition (APBC) is realized by applying a noncontractable loop of gauge symmetry operator $Z = \prod_i Z_i$ on the virtual space [15], where the gauge symmetry operator Z_i takes the form $Z_i = (-1)^{n_i}$, as illustrated in Fig. 3(b). Here, the gauge symmetry can be interpreted as the fermion parity of virtual spin-$\frac{1}{2}$ particles or the number parity of singlet pairs crossing the ith virtual bond [16,44]. The $SU(2)_1$ CSLs on the cylinder have two topological sectors. On a finite cylinder, the minimally entangled states (MESs) [45,46] are determined by explicitly controlling populations of edge modes in the unprojected states. Correspondingly, on the infinite cylinder we determine the MES according to the single-particle ES in the unprojected states as well as virtual space quantum numbers, based on the equivalence between the edge spectrum and ES, as implied by Eq. (2) [34,35].

To control the filling of the free fermion edge modes, we plot in Fig. 3(c) the spectrum of the subsystem correlation matrix representing a (single) physical edge. The Fermi level $\epsilon_F = 0.5$ ($\lambda_F = 0$ marked by a dashed line) defines the Fermi sea state $|\psi_{\rm FS}\rangle = \prod_{\sigma=\uparrow,\downarrow} \prod_{1-\epsilon_\alpha<\epsilon_F} d^\dagger_{\alpha,\sigma}|{\rm Vac}\rangle$, where $d^\dagger_{\alpha,\sigma}$ denote the bulk and edge modes with eigenvalue ϵ_α and spin

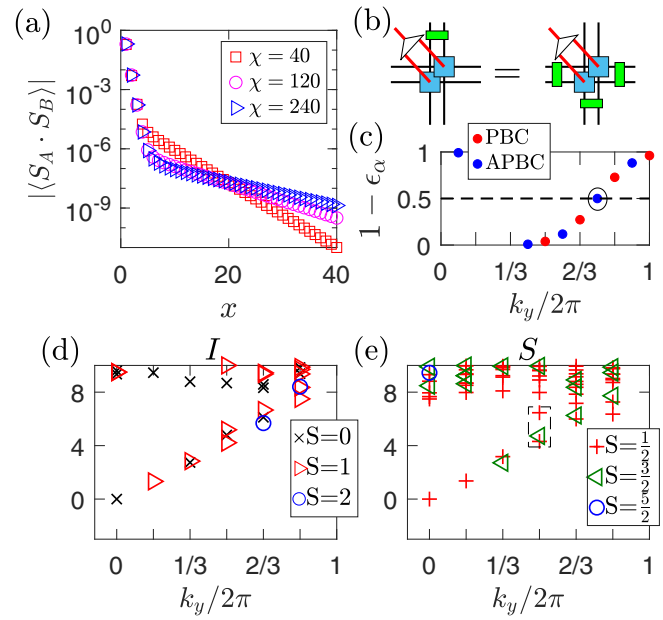

FIG. 3. Features of projected and unprojected $C = 1$ states obtained from optimizing the Hofstadter model at $t_2 = 0.5$ and $M = 2$. (a) Correlation functions after Gutzwiller projection, computed with various χ. (b) Gauge symmetry in the local tensor of the Gutzwiller projected state. (c) Edge spectrum of the free fermion correlation matrix on a width $N_y = 6$ cylinder with PBC and APBC. The dashed line denotes the Fermi level of the entanglement Hamiltonian. (d) and (e) Entanglement spectra of the identity (I) and semion (S) sectors in the Gutzwiller projected states on the width $N_y = 6$ cylinder with PBC and APBC, respectively. CTMRG boundary tensors with $\chi = 110$ are used. The contents of the ES match the theoretical expectations up to the fourth level, which are listed in the SM.

polarization σ. The $SU(2)_1$ ground states in identity (I) and semion (S) sectors can be constructed on the PBC/APBC cylinder as [47]

$$|\psi_I\rangle = P_G|\psi_{\rm FS}\rangle_{\rm PBC},$$
$$|\psi_S\rangle_{\sigma,\bar{\sigma}} = P_G \zeta^\dagger_{L,\sigma}\zeta^\dagger_{R,\bar{\sigma}}|\psi_{\rm FS}\rangle_{\rm APBC}, \quad (3)$$

respectively. Here, $\zeta^\dagger_{L/R,\sigma}$ creates the lowest particle excitation at the left/right boundary as marked by the black circle, and the superposition $|\psi_S\rangle_{\uparrow,\downarrow} - |\psi_S\rangle_{\downarrow,\uparrow}$ forms a singlet. The two topological sectors have a total spin difference $\Delta S = \frac{1}{2}$ in the horizontal virtual space and can be distinguished by the y-direction loop operator $P_{\rm even/odd} = (1 \pm Z)/2$ that projects to the subspaces of integer spin (even charge parity) and half-integer spin (odd charge parity) in the ES, respectively.

Figures 3(d)–3(e) show numerical results of the Gutzwiller projected state on the width $N_y = 6$ cylinder for I and S sectors obtained with PBC and APBC, respectively, where the entanglement Hamiltonians [48] are built from CTMRG boundary tensors [23,27,49]. Numerically, the integer (half-integer) sector corresponds to the fixed point of the transfer matrix with PBC (APBC), in agreement with the fact that, for both cases, the unprojected edge modes are half-filled [Fig. 3(c)]. The low-energy levels match the prediction of $SU(2)_1$ Wess-Zumino-Witten CFT (see SM [38]), including the one marked by the dashed rectangle. We notice that, in

contrast with the previous bosonic PEPS method [26,27], our fermionic construction yields the correct number of chiral branches in the ES. We also remark that we expect both sectors can be obtained within a fixed boundary condition if N_y is large enough with sufficient number of linear edge states, as in Fig. 2(b).

Gutzwiller projected spin states with $C = 2$. The above approach can be naturally generalized to parton states with arbitrary Chern number. Here, we consider a $C = 2$ model [50], which turns out to be nontrivial, as it shows that the topological order of a generic projected parton state depends not only on the Chern number before projection but also on details of the wave functions.

The family of free fermion $C = 2$ Hamiltonians H_Θ have A, B sublattices in the unit-cell. At $\Theta = 0$, it takes the form:

$$\begin{aligned} H_{\Theta=0} = & \sum_{\langle i,j\rangle_x} t_1 (c^\dagger_{j,A} c_{i,B} + c^\dagger_{j,B} c_{i,A}) \\ & + \sum_{\langle i,j\rangle_y} t_1 (c^\dagger_{j,A} c_{i,A} - c^\dagger_{j,B} c_{i,B}) \\ & + \sum_{\langle\langle i,k\rangle\rangle} t_2 \exp(2i\theta_{ik}) (c^\dagger_{k,B} c_{i,A} - c^\dagger_{k,A} c_{i,B}) \\ & + \text{H.c.}, \end{aligned} \tag{4}$$

where i, j, k denotes the sites on the x-y plane, and θ_{ik} denotes the angle between next-nearest-neighbor sites i, k. The model at $\Theta = 0$ can be viewed as two independent layers of Eq. (1) that differ by a one-site translation T_x along the x direction: By taking A sites for the even x coordinate and taking B sites for the odd x coordinate, one obtains the first copy, and vice versa for the second copy. Due to the T_x translation, the ESs along the y direction cut contributed from two layers are identical but have π momentum difference, as shown in Fig. 4(a) for optimized $M = 2$ GfPEPS with PBC and APBC (with a string along the x direction inserted), respectively. Applying the local unitary $U(\Theta) = \exp[\sum_i \Theta(c^\dagger_{i,A} c_{i,B} - c^\dagger_{i,B} c_{i,A})/2]$ that acts inside each unit-cell, the family of Hamiltonian $H_\Theta = U^{-1}(\Theta) H_0 U(\Theta)$ is obtained. At $\Theta = 0$, the two $C = 1$ layers are independent, and at $\Theta = \pi/4$, the two layers are maximally mixed. The total Chern number and free fermion ES do not depend on Θ since $U(\Theta)$ is local.

After Gutzwiller projection, a topological transition emerges along the path $\Theta \in [0, \pi/4]$ (see SM [38]). At $\Theta < \Theta_c$, the projected state is the Abelian $\mathrm{SU}(2)_1 \times \mathrm{SU}(2)_1$ since the $\Theta = 0$ gapped topological phase of the two decoupled layers should have a finite extension in parameter space. We focus on the $\mathrm{SO}(5)_1$ CSL realized around the maximally mixed limit $\Theta = \pi/4$ which was predicted by the effective field theory and verified recently by a matrix product state calculation [50,51]. Before investigating the topological properties of this non-Abelian CSL, we emphasize that correlations of the projected GfPEPS [Fig. 4(b)] show a similar crossover behavior as in Fig. 3(a), pointing toward the universality of such an artifact in chiral PEPSs.

In the free fermion edge spectrum on the left boundary of the $N_y = 6$ cylinder, we denote $\zeta^\dagger_{L,1,\sigma}, \zeta^\dagger_{L,2,\sigma}$ as the first excited states with momentum difference π marked by the black circles in Fig. 4(a) for both PBC and APBC. For the

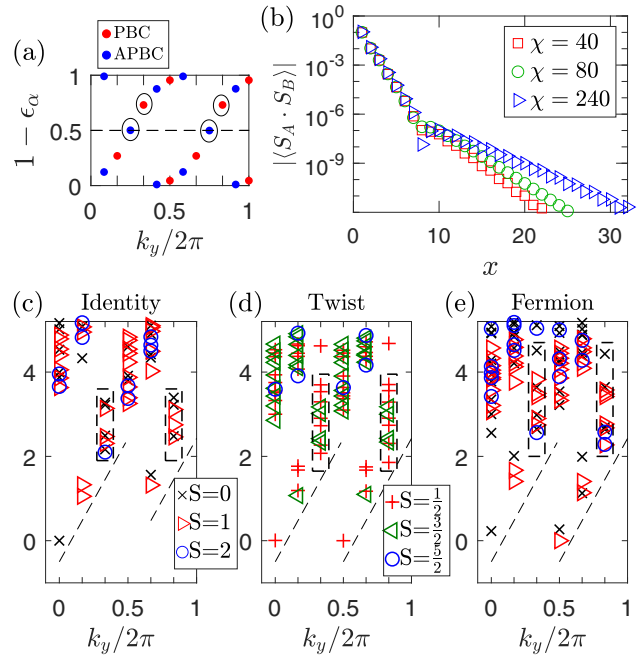

FIG. 4. Features of the unprojected and projected $C = 2$ states with $M = 2$ at $\Theta = \pi/4$. (a) Edge spectrum of the free fermion correlation matrix on a width $N_y = 6$ cylinder with PBC and APBC. (b) Correlation functions after Gutzwiller projection computed at different χ. [(c)–(e)] The ES of $\mathrm{SO}(5)_1$ CSL at $\Theta = \pi/4$ with CTMRG $\chi = 110$. In (c) and (e), PBC is used, and in (d), APBC is used. The contents of ES match theoretical expectations up to the third level, which are listed in the SM.

$\mathrm{SO}(5)_1$ CSL, three MESs [51] can be constructed as

$$\begin{aligned} |\psi_{\text{Identity}}\rangle &= P_G |\psi_{\text{FS}}\rangle_{\text{PBC}}, \\ |\psi_{\text{Twist}}\rangle_{\sigma,\bar{\sigma}} &= P_G \zeta^\dagger_{L,a,\sigma} \zeta_{R,a,\sigma} |\psi_{\text{FS}}\rangle_{\text{PBC}}, \\ |\psi_{\text{Fermion}}\rangle &= P_G \zeta^\dagger_{L,a,\uparrow} \zeta^\dagger_{L,a,\downarrow} \zeta^\dagger_{R,b,\uparrow} \zeta^\dagger_{R,b,\downarrow} |\psi_{\text{FS}}\rangle_{\text{APBC}}. \end{aligned} \tag{5}$$

Here, $a, b \in \{1, 2\}$. For the twist sector, due to the annihilation operator $\zeta_{R,a,\sigma}$, a single spin $\bar{\sigma}$ edge mode is left at the right boundary. The numerical results for the projected states at $\Theta = \pi/4$ are shown in Figs. 4(c)–4(e). With PBC and APBC, the dominant integer spin sectors which have half-filled edge modes are shown to be the identity and fermion sectors, respectively. The half-integer (odd charge parity) sector with PBC gives the twist sector. The $\Delta k_y = \pi$ momentum splitting of the chiral branches originates from the existence of two edge branches shifted by π before projection. A key advantage of the fermionic approach is that all topological sectors can be explicitly constructed, which is not obvious to achieve within the bosonic PEPS framework [23]. The level counting of the numerically obtained ES shows a remarkable agreement with the CFT prediction, which is given in the SM [38].

Conclusions. We have investigated the Gutzwiller-projected Chern insulators in the GfPEPS representation. The topological obstruction for chiral GfPEPS only leads to very weak Gossamer tails in the correlation functions of projected GfPEPSs and thus brings no practical obstruction for

numerical simulations. Within our framework, topological sectors can be tuned conveniently by flux insertion without explicit control of edge mode populations, and the projected GfPEPSs provide faithful descriptions of the edge spectra in both Abelian and non-Abelian CSLs, which would be interesting to further analyze via a recently proposed generalized Gibbs ensemble approach [52]. In the future, it would also be interesting to study frustrated spin models using projected GfPEPS as an initial variational *Ansatz*, where variational parameters are elements of on-site tensors. After optimization, the state is no longer a projected Gaussian state and becomes a general PEPS, but the proper ES countings are expected to be retained. Note that, without this parton construction, the direct variational optimization of bosonic PEPSs always yields *Ansätze* with redundant ES degeneracy. Note also that the non-Abelian $SO(5)_1$ CSL does not seem to have a simple description in terms of bosonic PEPSs. One natural question emerges: For spin systems, is there a difference in the representative power of bosonic PEPSs and fermion PEPSs? We leave this question to future research.

Acknowledgments. We thank Hong-Hao Tu for insightful discussions. We implemented non-Abelian symmetries using the TensorKit.jl package [53]. We were granted access to the HPC resources of the CALMIP center under the Allocation No. 2017-P1231. J.-Y.C. acknowledges support by Open Research Fund Program of the State Key Laboratory of Low-Dimensional Quantum Physics (Project No. KF202207), Fundamental Research Funds for the Central Universities, Sun Yat-sen University (Project No. 23qnpy60), a startup fund from Sun Yat-sen University, the Innovation Program for Quantum Science and Technology No. 2021ZD0302100, and National Natural Science Foundation of China (NSFC) (Grant No. 12304186). J.-W.L. acknowledges funding support from the Plan France 2030 ANR-22-PETQ-0007 "EPIQ". This letter was also supported by the ANR-18-CE30-0026-01 "TNTOP" grant awarded by the French Research Council.

[1] F. D. M. Haldane, Model for a quantum Hall effect without landau levels: Condensed-matter realization of the parity anomaly, Phys. Rev. Lett. **61**, 2015 (1988).
[2] X.-L. Qi and S.-C. Zhang, Topological insulators and superconductors, Rev. Mod. Phys. **83**, 1057 (2011).
[3] D. J. Thouless, M. Kohmoto, M. P. Nightingale, and M. den Nijs, Quantized Hall conductance in a two-dimensional periodic potential, Phys. Rev. Lett. **49**, 405 (1982).
[4] Y. Hatsugai, Chern number and edge states in the integer quantum Hall effect, Phys. Rev. Lett. **71**, 3697 (1993).
[5] X.-G. Wen, Quantum orders and symmetric spin liquids, Phys. Rev. B **65**, 165113 (2002).
[6] H. Li and F. D. M. Haldane, Entanglement spectrum as a generalization of entanglement entropy: Identification of topological order in non-Abelian fractional quantum Hall effect states, Phys. Rev. Lett. **101**, 010504 (2008).
[7] X.-L. Qi, H. Katsura, and A. W. W. Ludwig, General relationship between the entanglement spectrum and the edge state spectrum of topological quantum states, Phys. Rev. Lett. **108**, 196402 (2012).
[8] K. Gawedzki, Wess-Zumino-Witten conformal field theory, in *Constructive Quantum Field Theory II*, edited by G. Velo and A. S. Wightman (Springer US, Boston, 1990), pp. 89–120.
[9] V. Kalmeyer and R. B. Laughlin, Equivalence of the resonating-valence-bond and fractional quantum Hall states, Phys. Rev. Lett. **59**, 2095 (1987).
[10] Y. Zhang, T. Grover, and A. Vishwanath, Topological entanglement entropy of $\mathbb{Z}_2$ spin liquids and lattice Laughlin states, Phys. Rev. B **84**, 075128 (2011).
[11] R. B. Laughlin, Anomalous quantum Hall effect: An incompressible quantum fluid with fractionally charged excitations, Phys. Rev. Lett. **50**, 1395 (1983).
[12] F. Becca and S. Sorella, *Quantum Monte Carlo Approaches for Correlated Systems* (Cambridge University Press, Cambridge, UK, 2017).
[13] A. Anand, R. A. Patil, A. C. Balram, and G. J. Sreejith, Real-space entanglement spectra of parton states in fractional quantum Hall systems, Phys. Rev. B **106**, 085136 (2022).
[14] F. Verstraete and J. I. Cirac, Renormalization algorithms for quantum-many body systems in two and higher dimensions, arXiv:cond-mat/0407066.
[15] N. Schuch, I. Cirac, and D. Pérez-García, PEPS as ground states: Degeneracy and topology, Ann. Phys. **325**, 2153 (2010).
[16] N. Schuch, D. Poilblanc, J. I. Cirac, and D. Pérez-García, Resonating valence bond states in the PEPS formalism, Phys. Rev. B **86**, 115108 (2012).
[17] J.-Y. Chen and D. Poilblanc, Topological $\mathbb{Z}_2$ resonating-valence-bond spin liquid on the square lattice, Phys. Rev. B **97**, 161107(R) (2018).
[18] J. I. Cirac, D. Pérez-García, N. Schuch, and F. Verstraete, Matrix product states and projected entangled pair states: Concepts, symmetries, theorems, Rev. Mod. Phys. **93**, 045003 (2021).
[19] T. B. Wahl, H.-H. Tu, N. Schuch, and J. I. Cirac, Projected entangled-pair states can describe chiral topological states, Phys. Rev. Lett. **111**, 236805 (2013).
[20] T. B. Wahl, S. T. Haßler, H.-H. Tu, J. I. Cirac, and N. Schuch, Symmetries and boundary theories for chiral projected entangled pair states, Phys. Rev. B **90**, 115133 (2014).
[21] J. Dubail and N. Read, Tensor network trial states for chiral topological phases in two dimensions and a no-go theorem in any dimension, Phys. Rev. B **92**, 205307 (2015).
[22] D. Poilblanc, Investigation of the chiral antiferromagnetic Heisenberg model using projected entangled pair states, Phys. Rev. B **96**, 121118(R) (2017).
[23] J.-Y. Chen, L. Vanderstraeten, S. Capponi, and D. Poilblanc, Non-Abelian chiral spin liquid in a quantum antiferromagnet revealed by an iPEPS study, Phys. Rev. B **98**, 184409 (2018).
[24] S. Niu, J. Hasik, J.-Y. Chen, and D. Poilblanc, Chiral spin liquids on the kagome lattice with projected entangled simplex states, Phys. Rev. B **106**, 245119 (2022).
[25] J. Hasik, M. Van Damme, D. Poilblanc, and L. Vanderstraeten, Simulating chiral spin liquids with projected entangled-pair states, Phys. Rev. Lett. **129**, 177201 (2022).
[26] D. Poilblanc, J. I. Cirac, and N. Schuch, Chiral topological spin liquids with projected entangled pair states, Phys. Rev. B **91**, 224431 (2015).

[27] D. Poilblanc, N. Schuch, and I. Affleck, $SU(2)_1$ chiral edge modes of a critical spin liquid, Phys. Rev. B **93**, 174414 (2016).
[28] A. Hackenbroich, A. Sterdyniak, and N. Schuch, Interplay of SU(2), point group, and translational symmetry for projected entangled pair states: Application to a chiral spin liquid, Phys. Rev. B **98**, 085151 (2018).
[29] In Ref. [37], a SU(2) breaking chiral topological state constructed from a specific gapless topological superconductor was studied. In this letter, our scheme targets SU(2) symmetric chiral spin liquids constructed from generic chiral topological insulators with arbitrary Chern number.
[30] D. Wang, Z. Liu, J. Cao, and H. Fan, Tunable band topology reflected by fractional quantum Hall states in two-dimensional lattices, Phys. Rev. Lett. **111**, 186804 (2013).
[31] J.-Y. Chen, J.-W. Li, P. Nataf, S. Capponi, M. Mambrini, K. Totsuka, H.-H. Tu, A. Weichselbaum, J. von Delft, and D. Poilblanc, Abelian $SU(N)_1$ chiral spin liquids on the square lattice, Phys. Rev. B **104**, 235104 (2021).
[32] Q. Mortier, N. Schuch, F. Verstraete, and J. Haegeman, Tensor networks can resolve Fermi surfaces, Phys. Rev. Lett. **129**, 206401 (2022).
[33] J.-W. Li, J. von Delft, and H.-H. Tu, U(1)-symmetric Gaussian fermionic projected entangled paired states and their Gutzwiller projection, Phys. Rev. B **107**, 085148 (2023).
[34] I. Peschel, Calculation of reduced density matrices from correlation functions, J. Phys. A: Math. Gen. **36**, L205 (2003).
[35] A. M. Turner, Y. Zhang, and A. Vishwanath, Entanglement and inversion symmetry in topological insulators, Phys. Rev. B **82**, 241102(R) (2010).
[36] X.-L. Qi, Y.-S. Wu, and S.-C. Zhang, Topological quantization of the spin Hall effect in two-dimensional paramagnetic semiconductors, Phys. Rev. B **74**, 085308 (2006).
[37] S. Yang, T. B. Wahl, H.-H. Tu, N. Schuch, and J. I. Cirac, Chiral projected entangled-pair state with topological order, Phys. Rev. Lett. **114**, 106803 (2015).
[38] See Supplemental Material at http://link.aps.org/supplemental/10.1103/PhysRevB.109.L081107 for results for optimized Gf-PEPSs from other Chern insulator models, predicted level countings for relevant CSLs, and ES evolution across the topological transition of the Gutzwiller projected $C = 2$ parton wave functions.
[39] T. Barthel, C. Pineda, and J. Eisert, Contraction of fermionic operator circuits and the simulation of strongly correlated fermions, Phys. Rev. A **80**, 042333 (2009).
[40] P. Corboz, R. Orús, B. Bauer, and G. Vidal, Simulation of strongly correlated fermions in two spatial dimensions with fermionic projected entangled-pair states, Phys. Rev. B **81**, 165104 (2010).
[41] T. Nishino and K. Okunishi, Corner transfer matrix renormalization group method, J. Phys. Soc. Jpn. **65**, 891 (1996).
[42] P. Corboz, T. M. Rice, and M. Troyer, Competing states in the *t-J* model: Uniform *d*-wave state versus stripe state, Phys. Rev. Lett. **113**, 046402 (2014).
[43] N. Schuch, D. Poilblanc, J. I. Cirac, and D. Perez-Garcia, Topological order in the projected entangled-pair states formalism: Transfer operator and boundary Hamiltonians, Phys. Rev. Lett. **111**, 090501 (2013).
[44] D. Poilblanc, N. Schuch, D. Pérez-García, and J. I. Cirac, Topological and entanglement properties of resonating valence bond wave functions, Phys. Rev. B **86**, 014404 (2012).
[45] Y. Zhang, T. Grover, A. Turner, M. Oshikawa, and A. Vishwanath, Quasiparticle statistics and braiding from ground-state entanglement, Phys. Rev. B **85**, 235151 (2012).
[46] H.-H. Tu, Y. Zhang, and X.-L. Qi, Momentum polarization: An entanglement measure of topological spin and chiral central charge, Phys. Rev. B **88**, 195412 (2013).
[47] Y.-H. Wu, L. Wang, and H.-H. Tu, Tensor network representations of parton wave functions, Phys. Rev. Lett. **124**, 246401 (2020).
[48] J. I. Cirac, D. Poilblanc, N. Schuch, and F. Verstraete, Entanglement spectrum and boundary theories with projected entangled-pair states, Phys. Rev. B **83**, 245134 (2011).
[49] J.-Y. Chen, S. Capponi, A. Wietek, M. Mambrini, N. Schuch, and D. Poilblanc, $SU(3)_1$ chiral spin liquid on the square lattice: A view from symmetric projected entangled pair states, Phys. Rev. Lett. **125**, 017201 (2020).
[50] Y. Zhang and X.-L. Qi, Identifying non-Abelian topological ordered state and transition by momentum polarization, Phys. Rev. B **89**, 195144 (2014).
[51] Y.-H. Wu and H.-H. Tu, Non-Abelian topological order with $SO(5)_1$ chiral edge states, Phys. Rev. B **106**, 115129 (2022).
[52] M. J. Arildsen and A. W. W. Ludwig, Generalized Gibbs ensemble description of real-space entanglement spectra of $(2+1)$-dimensional chiral topological systems with SU(2) symmetry, Phys. Rev. B **106**, 035138 (2022).
[53] J. Haegeman, TensorKit.jl: A Julia package for large-scale tensor computations, with a hint of category theory, https://github.com/Jutho/TensorKit.jl.